Equivalent Circuit Formulation for Solving AC Optimal Power Flow

Marko Jereminov, *Member, IEEE*, Amritanshu Pandey, *Graduate Student Member, IEEE*, and Larry Pileggi, *Fellow, IEEE*

***Abstract*—In this paper, we formulate and solve the ac optimal power flow (AC-OPF) as an equivalent circuit problem in terms of current, voltage, and admittance state variables. The generator models are represented using conductance and susceptance state variables, and the operational and network constraints are translated to corresponding current/voltage constraints without loss of accuracy or generality. To understand the physics behind the optimality conditions of the optimization problem, we extend the linear adjoint circuit theory to translate them to equivalent circuit domain. It is shown that the operating point that defines the equivalent circuit solution precisely represents an AC-OPF solution. We then further exploit the equivalent circuit representation to use power flow simulation techniques to robustly solve the optimization problem. The efficiency of our approach is demonstrated for several AC-OPF benchmark test cases (up to 70 k buses) under nominal and congested operating conditions, and the runtime and scalability properties are presented.**

***Index Terms*—AC optimal power flow, equivalent circuit, circuit formulation, circuit formalism, nonlinear optimization.**

I. Introduction

THE AC Power Flow analysis, based on iteratively solving the nonlinear power mismatch equations, was first conceived five decades ago [1], and still remains the standard analysis for operation and planning of the transmission-level power grids. Not long after the first power flow formulation was postulated, the Alternating Current Optimal Power Flow (AC-OPF) was introduced by Carpentier [2] and Dommel and Tinney in [3]. The motivation behind the first AC-OPF problem was to find a steady-state operating point of a power system that minimizes the cost of generated real power while satisfying the operating, network and stability constraints. Most notably, the financial market is defined by nonlinear pricing, while the highly nonlinear 'PQV' based power mismatch equations characterize the network constraints that model the electrical power system [4]. When both are combined with operating and stability constraints, they create a daunting optimization problem with many possible local optimal solutions [5]. For this reason, the classical OPF is recognized as a NP hard problem to solve, and a robust technique that can solve for *an* optimal solution in a reasonable amount of time still does not exist [4]. FERC (Federal Energy Regulatory Commission) has reported [4] that today's "approximate-solution techniques may unnecessarily cost tens of billions of dollars per year" and "result in environmental harm from unnecessary emissions."

Developing the robust and efficient methodology that can solve for an optimal solution of the AC-OPF problem has been a prominent research challenge and was until recently based on improving the local optimization algorithms [6]. The recent breakthrough has been made by introduction of relaxation algorithms that claim to find the global optimal solution of AC-OPF in [7]–[11]. The most promising advancement is presented in [8], [9], where the authors use the Semi-Definite (SDP) and Second-Order Cone (SOCP) Programing relaxation to handle the non-convexities of the AC-OPF problem. The proposed relaxation algorithms are demonstrated to be exact and yield the zero-duality gap for the initially examined test cases [8]. Unfortunately, this is not the case in general [5], [12], and as discussed in [5], the proposed SDP/SOCP relaxations succeed in solving radial network configuration test cases but are exact for meshed network test cases when there is only one feasible solution [5], [12]. The other major drawbacks that further affect the recovery of the global optimum from the relaxed problems, such as the inability to handle negative Lagrange multipliers caused by bounding line constraints, are discussed in [12].

Understanding and exploiting the physics of a power system is the key factor to robust simulation and relaxation algorithms [10]. Importantly, the inherent nonlinearity of the traditionally used 'PQV' formulation due to the power mismatch equations represent the biggest impediment to the formulation and efficient solution [4]. Therefore, different formulations that have been proposed since the introduction of AC-OPF problem mostly differ in the approaches used to characterize the network constraints [4]. Notably, it has been suggested [4] that the current-voltage based (*I-V*) formulations with linear network constraints and local nonlinearities isolated at each bus, seemingly represents the most promising formulation for modeling of network constraints. However, efficient handling of generator models that has previously shown to be challenging for *I-V* formulations of transmission level powerflow simulations [13], [14] worsened in the optimization problem, causing numerical

Manuscript received July 1, 2018; revised September 20, 2018 and November 12, 2018; accepted December 15, 2018. Date of publication December 20, 2018; date of current version April 17, 2019. This work was supported in part by the Defense Advanced Research Projects Agency under Award FA8750-17-1-0059 for the RADICS program and in part by the National Science Foundation under Contract ECCS-1800812. Paper no. TPWRS-01004-2018. *(Corresponding author: Marko Jereminov.)*

The authors are with the Department of Electrical and Computer Engineering, Carnegie Mellon University, Pittsburgh, PA 15213 USA (e-mail: mjeremin@andrew.cmu.edu; amritanp@andrew.cmu.edu; pileggi@andrew.cmu.edu).

Color versions of one or more of the figures in this paper are available online at http://ieeexplore.ieee.org.

Digital Object Identifier 10.1109/TPWRS.2018.2888907

instability to occur [14]. To address this, the authors in [14] have proposed the hybrid method, where the generator buses are modeled using power mismatch equations while the rest of the network is handled using current mismatch equations. Importantly, this and all of the proposed formulations are based on the models that introduce other non-convexities in both the equality and inequality constraints. This keeps the OPF problem highly nonlinear, as well as prevents the robust large-scale optimization of power systems due to the inability to efficiently handle the nonlinear constraints [4]. Therefore, the challenge remains to find a robust algorithm that is capable of solving the generalized AC-OPF problem with all the emerging and existing grid technologies.

Recent advances in power system simulations have included the use of complex current and voltage state variables within the equivalent split-circuit framework for solving the powerflow [15]–[17]. This formulation has demonstrated that the equivalent circuit formalism provides new insight into robustly analyzing the complete powerflow simulation problem [16]. More importantly, decades of research toward advancing circuit simulation methods that are now capable of robustly simulating nonlinear circuits with billions of nodes can be adapted and directly applied to the analysis of power systems [18]. Thus, it is shown that the generator model problems introduced by application of the *I-V* formulation can be successfully overcome, thereby allowing the robust scaling to massive-size transmission problems [17].

In this paper we propose a novel framework for solving the AC Optimal Power Flow problem in terms of equivalent split-circuit state variables as an extension of the recent advancements in power flow analysis. The key contribution of the paper is the representation of the AC-OPF problem in terms of a nonlinear equivalent circuit problem. Importantly, the generator model is redefined (Section III) in terms of conductance and susceptance state variables, where the negative conductance supplies the real power to the circuit, while the susceptance represents an inductor or capacitor that supplies or absorbs the reactive power respectively. The objective of real power cost minimization is now related to the network constraints through the generator admittance state variables. This formulation does not encounter the convergence problems as reported for existing *I-V* formulations [14].

As part of this formulation, a significant contribution is attributed to extending the theory for linear adjoint (dual) circuits to modeling the steady-state nonlinearities at fixed frequency introduced by constant power models. We derive the adjoint circuits for constant power models in Section IV, and further show that coupled simulation of power flow and its adjoint circuit with addition of other control circuits exactly maps the necessary optimality conditions of the optimization problem. Therefore, if sufficient conditions are met, the circuit solution exactly represents an optimal power flow solution.

Lastly, a supporting contribution is the development of circuit simulation techniques to ensure the robust large-scale convergence of proposed circuit formulation. The overall result is our algorithm, ESCAPE (Enhanced Simulation of Circuit-based AC-OPF Problem Equivalent), that is an extension of our recently introduced powerflow circuit simulation methods [16], [17], with inclusion of diode limiting heuristics [20], [21] to preserve the robust and efficient convergence properties, scalable to any-size power grids.

The proposed framework is applied to solve the AC-OPF circuit for congested and nominal (without congestion constraints) operating conditions of various available test cases (up to 70 k buses), and the results are compared with traditional AC-OPF and SDP relaxed AC-OPF results in Section VI.

II. Traditional AC-OPF Formulations

Consider a power system given by the set of buses $\mathcal{N}$, whereas set of generators $\mathcal{G}$ and load demands $\mathcal{D}$ are subsets of $\mathcal{N}$, that are further connected by a set of network elements, $\mathcal{T}_X$. The objective of traditional AC-OPF is to find a steady-state solution of a power system that minimizes the cost function of real power generation, $\mathcal{F}_c(\boldsymbol{P_G})$, defined throughout the paper as a quadratic function given by a set of coefficients $\{\boldsymbol{a}, \boldsymbol{b}, \boldsymbol{c}\}$:

$$\min_{\boldsymbol{P_G}} \mathcal{F}_c\left(\boldsymbol{P_G}\right) = \sum_{g=1}^{|\mathcal{G}|} \left[a_g + b_g P_{G,g} + c_g P_{G,g}^2\right] \tag{1}$$

while satisfying the power balance equations (2), (3) and additional operational constraints (4)–(7).

$$P_{G,(g\in\mathcal{G}(i))} - P_{D,i} = |V_i| \sum_{k=1}^{|\mathcal{N}|} |V_k| \left(G_{ik}^Y \cos\theta_{ik} + B_{ik}^Y \sin\theta_{ik}\right) \tag{2}$$

$$Q_{G,(g\in\mathcal{G}(i))} - Q_{D,i} = |V_i| \sum_{k=1}^{|\mathcal{N}|} |V_k| \left(G_{ik}^Y \sin\theta_{ik} - B_{ik}^Y \cos\theta_{ik}\right) \tag{3}$$

$$P_{min,g} \le P_{G,g} \le P_{max,g} \qquad \forall g \in \mathcal{G} \tag{4}$$

$$Q_{min,g} \le Q_{G,g} \le Q_{max,g} \qquad \forall g \in \mathcal{G} \tag{5}$$

$$V_{min,i} \le |V_i| \le V_{max,i} \qquad \forall i \in \mathcal{N} \tag{6}$$

$$P_e^2 + Q_e^2 \le S_{max,e}^2 \qquad \forall e \in \mathcal{T}_X \tag{7}$$

where $|V_i|$ and θ_i represent voltage magnitude and angle state variables, whereas $P_{G,(g\in\mathcal{G}(i))}$, $P_{D,i}$, $Q_{G,(g\in\mathcal{G}(i))}$ and $Q_{D,i}$ are generated and demanded real and reactive powers at the ith bus respectively. Variable θ_{ik} defines the voltage angle difference between buses i and k, while G_{ik}^Y and B_{ik}^Y represent the real and imaginary parts of the bus admittance matrix. Each generator in the set $\mathcal{G}$ is further defined by the operating bounds on real and reactive powers ($P_{min,\,g}$, $P_{max,\,g}$, $Q_{min,\,g}$ and $Q_{max,\,g}$) given in (4) and (5), while the voltage magnitude of each bus is bounded by the operating limits given in (6). Lastly, (7) represents the thermal limits of a eth network branch, given for maximum apparent power flow bounds ($S_{max,e}$), where real and reactive power flows can be written as functions of ith and kth bus voltage magnitudes and angles connected by the

branch e as:

$$P_e = |V_i|^2 G_{ik}^Y - |V_i|\,|V_k|\left(G_{ik}^Y \cos\theta_{ik} + B_{ik}^Y \sin\theta_{ik}\right) \quad (8)$$

$$Q_e = -|V_i|^2 B_{ik}^Y - |V_i|\,|V_k|\left(B_{ik}^Y \cos\theta_{ik} - G_{ik}^Y \sin\theta_{ik}\right) \quad (9)$$

It is important to note that the AC-OPF problem formulated using the power mismatch equations in rectangular coordinates seems to provide a less nonlinear (quadratic nonlinearities) formulation, and as such, is used for the relaxation approaches that are proposed in [7]–[11]. It does, however, preserve the local optimal solutions [5] and remains nonlinear and non-convex both locally and within the network configuration that has a linear nature in terms of current and voltage state variables (linear RLC network) [4].

III. Defining Network and Operational Constraints Using Equivalent Circuit State Variables

The equivalent circuit approach to generalized modeling of power flow was recently introduced in [15]–[17]. It was shown that each of the power system components can be translated to an equivalent circuit model based on underlying relations between current and voltage state variables without loss of generality. To further ensure the analyticity of nonlinear complex governing circuit equations for solution via Newton Raphson, the equations are split into real and imaginary parts and represented by two equivalent sub-circuits, real and imaginary, that are coupled by controlled sources. The equivalent split-circuit representation of the most prominent powerflow models are described in [15], [16].

In this section we rederive the circuit model of a generator based on the relationship between current, voltage and impedance, as well as introduce the transmission line congestion constraint based on maximum current limit. The two new models incorporated within the powerflow split-circuit formulation define the network constraints of the circuit theoretic AC-OPF problem.

A. Generator GB Macro-Model

Considering the $\tilde{V}_\Gamma$ and $\tilde{I}_{G,g}$ as the output complex voltage and complex current of the gth generator from the set $\mathcal{G}$, operating at a fundamental frequency, where the subscript index Γ represents the corresponding bus index of the gth generator.

For any operating point of a power system, there must exist a driving point admittance that completely characterizes the current and voltage relationship of that generator. Hence, a first order equivalent circuit model defined by a conductance that supplies the real power (a negative conductance) and a susceptance that adjusts the reactive power can completely capture such characteristics without loss of generality. The governing equation of the generator, whose equivalent circuit can be seen in Fig. 1(a), is obtained from Ohm's Law:

$$\tilde{I}_{G,g} = \left(G_{G,g} + jB_{G,g}\right)\tilde{V}_\Gamma \quad \forall g \in \mathcal{G} \quad (10)$$

The generated real and reactive powers ($P_{G,g}$, $Q_{G,g}$) are then constrained as given in (11), (12) and used to relate the equivalent circuit governing equations to the cost function of the optimization problem.

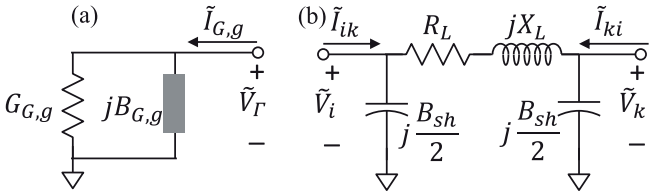

Fig. 1. (a) Macro-model of a generator in terms of conductance and susceptance state variables and (b) complex pi model of a transmission line.

$$P_{G,g} = -G_{G,g}|V_\Gamma|^2 \quad \forall g \in \mathcal{G} \quad (11)$$

$$Q_{G,g} = B_{G,g}|V_\Gamma|^2 \quad \forall g \in \mathcal{G} \quad (12)$$

B. Modeling the Voltage Magnitude Constraint

It can be shown that the voltage magnitude variable only appears as a squared term in the definitions of real and reactive powers, (11), (12). Therefore, to further control the bus voltage magnitudes within the optimization problem, we introduce a new variable, $d_{sq,i}$ that replaces the '$|V_i|^2$' term and further reduces the nonlinearities of the formulation. The voltage magnitude constraint and its limits are then redefined as:

$$d_{sq,i} = V_{R,i}^2 + V_{I,i}^2 \quad \forall i \in \mathcal{N} \quad (13)$$

$$V_{min,i}^2 \le d_{sq,i} \le V_{max,i}^2 \quad \forall i \in \mathcal{N} \quad (14)$$

Therefore, the generator real and reactive power constraints from (11), (12) are reformulated in terms of conductance, susceptance and d_{sq} variables, as follows:

$$P_{G,g} = -G_{G,g} d_{sq,\Gamma} \quad \forall g \in \mathcal{G} \quad (15)$$

$$Q_{G,g} = B_{G,g} d_{sq,\Gamma} \quad \forall g \in \mathcal{G} \quad (16)$$

The operating limits on real and reactive powers generated remain the same, as in (4) and (5).

Similarly, the PQ load split-circuit model [15], [16] connected to bus i, is reformulated in terms of d_{sq} as nonlinear real and imaginary current sources ($I_{PQ,i}^R$, $I_{PQ,i}^I$):

$$I_{PQ,i}^R = \frac{P_{L,i}}{d_{sq,i}} V_{R,i} + \frac{Q_{L,i}}{d_{sq,i}} V_{I,i} \quad \forall i \in (\mathcal{D} \subseteq \mathcal{N}) \quad (17)$$

$$I_{PQ,i}^I = \frac{P_{L,i}}{d_{sq,i}} V_{I,i} - \frac{Q_{L,i}}{d_{sq,i}} V_{R,i} \quad \forall i \in (\mathcal{D} \subseteq \mathcal{N}) \quad (18)$$

where $P_{L,i}$ and $Q_{L,i}$ are specified PQ load parameters, $V_{R,i}$ and $V_{I,i}$ are real and imaginary load voltages respectively.

C. Thermal Transmission Line Constraint

Traditional AC-OPF defines the transmission line thermal constraint as the upper bound of the apparent power flowing in the line, as in (7). However, the transmission line thermal constraints are determined by material properties of the transmission line conductors and equipment in terms of maximum current magnitude [4]. Therefore, constraining the current flow represents the most natural way of modeling this constraint.

Herein we show the thermal limit of a transmission line segment between nodes i and k, from Fig. 1(b), can be mapped to the equivalent maximum current limit and thereby trivially handled within the equivalent split-circuit framework. Thermal line constraint given in terms of the real and imaginary line currents can be expressed from the nominal voltage magnitude as:

$$I_{Rx,ik}^2 + I_{Ix,ik}^2 = i_{sq,ik} \leq \frac{S_{max,e}^2}{V_{nom}^2} \; \forall i,k \in \mathcal{N} \quad \forall e \in \mathcal{T}_X \tag{19}$$

The real and imaginary transmission line currents ($I_{Rx,ik}$ and $I_{Ix,ik}$) are further defined in terms of real and imaginary bus voltages:

$$I_{Rx,ik} = -\frac{B_{sh}}{2} V_{I,i} + G_L \left(V_{R,i} - V_{R,k}\right) - B_L \left(V_{I,i} - V_{I,k}\right) \tag{20}$$

$$I_{Ix,ik} = \frac{B_{sh}}{2} V_{R,i} + G_L \left(V_{I,i} - V_{I,k}\right) + B_L \left(V_{R,i} - V_{R,k}\right) \tag{21}$$

where $G_L = \dfrac{R_L}{R_L^2 + X_L^2}$ and $B_L = \dfrac{-X_L}{R_L^2 + X_L^2}$.

Alternatively, the thermal limit can be directly defined by the upper bound on current magnitude [4].

IV. Formulating Equivalent Split-Circuit Models of the AC-OPF Problem

A. Defining the Reformulated Optimization Problem

Consider the AC-OPF problem formulated in terms of power and our equivalent circuit state variables ($\boldsymbol{X}$):

$$\min_{\boldsymbol{P_G}} \mathcal{F}_c \left(\boldsymbol{P_G}\right) \tag{22}$$

subject to:

$$I_o \left(\boldsymbol{X}\right) \leq 0 \tag{23}$$

$$I_c \left(\boldsymbol{X}\right) = 0 \tag{24}$$

where

$$\boldsymbol{X} = \left[\boldsymbol{V_R}, \boldsymbol{V_I}, \boldsymbol{d_{sq}}, \boldsymbol{G}, \boldsymbol{B}, \boldsymbol{P_G}, \boldsymbol{Q_G}, \boldsymbol{i_{sq}}\right]^T \tag{25}$$

the bounds in (23) represent the operating limits of the power system defined in (4), (5), (15) and (19), while the set generalized circuit equations from (24) is given as:

$$\boldsymbol{G} \odot \boldsymbol{V_R} - \boldsymbol{B} \odot \boldsymbol{V_I} + \boldsymbol{I_{PQ}^R} + G^Y \boldsymbol{V_R} - B^Y \boldsymbol{V_I} = 0 \tag{26}$$

$$\boldsymbol{G} \odot \boldsymbol{V_I} + \boldsymbol{B} \odot \boldsymbol{V_R} + \boldsymbol{I_{PQ}^I} + G^Y \boldsymbol{V_I} + B^Y \boldsymbol{V_R} = 0 \tag{27}$$

$$\boldsymbol{P_G} + \boldsymbol{G} \odot \boldsymbol{d_{sq}} = 0 \tag{28}$$

$$\boldsymbol{Q_G} - \boldsymbol{B} \odot \boldsymbol{d_{sq}} = 0 \tag{29}$$

$$\boldsymbol{V_R} \odot \boldsymbol{V_R} + \boldsymbol{V_I} \odot \boldsymbol{V_I} - \boldsymbol{d_{sq}} = 0 \tag{30}$$

$$\boldsymbol{I_{Rx}} \odot \boldsymbol{I_{Rx}} + \boldsymbol{I_{Ix}} \odot \boldsymbol{I_{Ix}} - \boldsymbol{i_{sq}} = 0 \tag{31}$$

Herein, operator $\odot$ represents the Hadamard product, G^Y and B^Y represent the linear network given in terms of real and imaginary components of the bus admittance matrix, while the nonlinear PQ load currents ($\boldsymbol{I_{PQ}^R}, \boldsymbol{I_{PQ}^I}$) are functions of voltage variables as defined by (17), (18). Note that the conductance and susceptance ($\boldsymbol{G}$ and $\boldsymbol{B}$) represent the variable vectors with zero elements, corresponding to indices that are not in $\mathcal{G}$.

We start the derivation of the necessary optimality conditions by writing the Lagrangian function as:

$$\mathcal{L}\left(\boldsymbol{X}, \boldsymbol{\lambda}, \boldsymbol{\mu}\right) = \mathcal{F}_c + \boldsymbol{\lambda}^T I_c \left(\boldsymbol{X}\right) + \boldsymbol{\mu}^T I_o \left(\boldsymbol{X}\right) \tag{32}$$

Since the governing split-circuit equations are the real-valued functions continuous on the feasible domain, the primal, dual and complementary slackness (CS) problems, namely Karush-Kuhn-Tucker (KKT) conditions, are obtained by differentiating (32) with respect to primal and dual variables as:

$$\mathcal{J}_C^T \left(\boldsymbol{X}\right) \boldsymbol{\lambda} = -\nabla_{\boldsymbol{X}} \mathcal{F}_c - \mathcal{J}_o^T \boldsymbol{\mu} \tag{33}$$

$$I_c \left(\boldsymbol{X}\right) = 0 \tag{34}$$

$$\boldsymbol{\mu^T} I_o \left(\boldsymbol{X}\right) = 0 \tag{35}$$

$$I_o \left(\boldsymbol{X}\right) \leq 0 \tag{36}$$

$$\boldsymbol{\mu} \geq 0 \tag{37}$$

where $\mathcal{J}_C\left(\boldsymbol{X}\right)$ and $\mathcal{J}_o$ represent the Jacobian matrices of vector-valued functions $I_c(\boldsymbol{X})$ and $I_o(\boldsymbol{X})$, while $\nabla_{\boldsymbol{X}} \mathcal{F}_c$ is the gradient vector of the cost function $\mathcal{F}_c$.

Finally, the first order sensitivity matrix of the equivalent circuit constraints $\mathcal{J}_C(\boldsymbol{X})$ is dependent on $\boldsymbol{X}$, and therefore a solution to the redefined optimization problem ($\boldsymbol{X}^*$) is said to be optimal if in addition to satisfying the regulatory KKT conditions from (33)–(37), it further satisfies the second order sufficient condition [19] given by:

$$\boldsymbol{\tau}^T \frac{\partial \mathcal{J}^T \left(\boldsymbol{X}^*\right)}{\partial \boldsymbol{X}} \boldsymbol{\tau} > 0 \quad \forall \left(\boldsymbol{\tau} \neq 0\right) \in T_{X^*} \tag{38}$$

where T_{X^*} represents the tangent linear sub-space at $\boldsymbol{X}^*$.

To solve for the stationary point of KKT conditions ($\boldsymbol{X}^*$), there exist many algorithms that can be found in literature. One of them is the Primal-Dual Interior Point (PDIP) method [19], which approximates the complementary slackness condition from (35) as in (39), and iteratively solves the linearized (first order Taylor expansion) set of equations from (33), (34), (39).

$$\boldsymbol{\mu} \odot I_o \left(\boldsymbol{X}\right) = -\varepsilon \boldsymbol{e} \tag{39}$$

where the average complementary slackness violation (ε) approaches zero at convergence and $\boldsymbol{e}$ is vector of ones.

B. Translating Optimization Problem to Nonlinear Circuit Problem

The circuit theoretic formulation for modeling the network constraints of AC-OPF problem remains nonlinear due to the models that define the constant power elements, hence introduced the nonlinearities within the dual problem (33). Importantly, the generalized nonlinear optimization algorithms such as PDIP method, do not fully utilize the physics of the primal and dual AC-OPF nonlinearities, but apply the different types of generalized backtracking and damping techniques to ensure

feasibility and help convergence [19]. In contrast, the robust and scalable nonlinear simulation algorithms are developed from an understanding of the physics behind each nonlinear element within the problem. For instance, it would be intractable to use generalized nonlinear solvers to simulate a billion-node integrated circuit with nonlinearities such as diodes and transistors without utilizing knowledge of the physical device characteristics as done by SPICE, [20], [21].

We have recently demonstrated that the circuit formalism enabled within the equivalent split-circuit of a powerflow offers a new insight to understanding the knowledge of the physical characteristics of power grid device models. For instance, from the circuit perspective, the reported convergence instabilities reported in [14] for the generator model that is used for current injection based *I-V* formulations for power flow can be partially attributed to managing the set of constraints that control the voltage across the independent current sources [18]. This insight regarding the grid device characteristics can be utilized to ensure robust convergence along with scalability to any-size power flow problems [16], [17]. Hence, the same circuit simulation heuristics can be applied to the primal problem from (34). Herein, our objective is to *understand the nature of nonlinearities of dual problem* (33) *by representing it as an equivalent circuit* and solve it as a circuit simulation problem as well. The mapping doesn't introduce any approximation, but rather provides the important information that can be used in developing the circuit simulation heuristics solely based on the physics of the AC-OPF dual problem to enable robust convergence and scalability.

Adjoint (dual) linear circuit theory has been well studied and understood in the circuit modeling community and has been used for various circuit analyses, most notably noise analysis in SPICE [20]–[22]. It has been shown that every circuit element is further defined by the corresponding adjoint element in the dual domain [21], [22]. This mapping from primal to adjoint circuit domain is usually derived from Tellegen's Theorem and calculus of variations, however, due to the lack of circuit models that exhibit the constant steady-state power behavior, it has not been explored for the nonlinearities at fixed frequency. Therefore, to allow the circuit representation of dual problem from (33), we first extend the linear adjoint circuit theory to include the nonlinearities at fixed frequency.

Consider a primal time invariant circuit $\mathcal{C}$ and its topologically equivalent adjoint (dual) $\tilde{\mathcal{C}}$, as defined in phasor domain for a fixed frequency. To ensure the analyticity of complex circuits and their governing equations, we can without loss of generality split them into the respective real and imaginary sub-circuits, $\mathcal{S}$ and $\tilde{\mathcal{S}}$. Now, let the I, X, $\mathfrak{T}$ and λ represent the real valued branch current and state variables that fully define the primal and adjoint split-circuits respectively. From Tellegen's Theorem, in the most general form we can then write the following equivalent relationships [18], [21], [22]:

$$\boldsymbol{I}^T \boldsymbol{\lambda} = 0 \tag{40}$$

$$\boldsymbol{X}^T \boldsymbol{\mathfrak{T}} = 0 \tag{41}$$

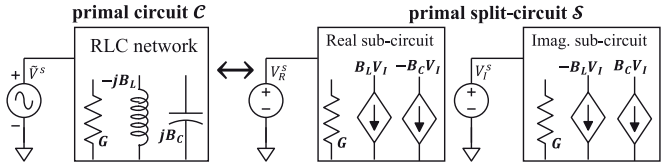

Fig. 2. n-node linear RLC circuit example.

The generalized governing equations of primal split-circuit $\mathcal{S}$ can be defined in terms of a sensitivity matrix $\mathcal{J}_X$:

$$\boldsymbol{I_c} = \mathcal{J}_X \ \boldsymbol{X} \tag{42}$$

where vector $\boldsymbol{I_c}$ defines the branch circuit currents and excitation sources that set the circuit operating point. Note that $\mathcal{J}_X$ of a liner split-circuit $\mathcal{S}$ represent a linear matrix given by the network conductance/susceptance values, while the nonlinear circuit elements (e.g., PQ load) additionally introduce the $\boldsymbol{X}$ dependent elements within $\mathcal{J}_X$.

If the generalized primal circuit equations from (42) are substituted for the branch currents $\boldsymbol{I}$ in (40), we obtain:

$$\boldsymbol{X}^T \mathcal{J}_X^T \boldsymbol{\lambda} = 0 \tag{43}$$

Hence, by comparing the (41) and (43), in order for Tellegen's Theorem to remain satisfied, the vector of adjoint currents $\boldsymbol{\mathfrak{T}}$ that further defines the generalized transformation from network $\mathcal{S}$ to its adjoint $\tilde{\mathcal{S}}$ has to correspond to:

$$\boldsymbol{\mathfrak{T}} = \mathcal{J}_X^T \boldsymbol{\lambda} \tag{44}$$

It can be inferred from (44), that the linear primal split-circuit corresponds to the respective linear adjoint circuit, while the nonlinear elements from the primal circuit $\mathcal{S}$ also introduce nonlinearities within the adjoint circuit $\tilde{\mathcal{S}}$. Interestingly, from the mathematical perspective, the sensitivity matrix that relates the adjoint currents and state variables also represents the dual matrix of $\mathcal{J}_X$.

To further clarify the mapping from primal to adjoint split circuits, we consider an n-node RLC network excited by a single fixed frequency voltage source, as shown in Fig. 2.

As can be seen from Fig. 2, we split the primal complex circuit (left) into the intercoupled real and imaginary sub-circuits (right). Note that the governing equations of the obtained sub-circuits correspond to the split real and imaginary parts of complex equations defining circuit $\mathcal{C}$. Hence, we write the sensitivity (split-admittance) matrix $\mathcal{J}_{X,RLC}$ in terms of conductance, and inductor and capacitor susceptance elements:

$$\mathcal{J}_{X,RLC} = \begin{bmatrix} \boldsymbol{G} & \boldsymbol{B_L - B_C} \\ \boldsymbol{B_C - B_L} & \boldsymbol{G} \end{bmatrix} \tag{45}$$

By further applying the primal to adjoint circuit mapping defined in (44), we can see that the dual RLC circuit represents nothing else but the complex conjugate of the primal one. For instance, a capacitive susceptance becomes inductive (conjugated), etc. The relationship between the RLC circuit elements in primal and adjoint domain, as well as constant power elements, is further summarized in Table I.

TABLE I
MAPPING OF CIRCUIT ELEMENTS TO DUAL DOMAIN

Primal circuit - $\mathcal{S}$		Adjoint circuit - $\widetilde{\mathcal{S}}$
Capacitor	$\leftrightarrow$	Inductor
Conductance	$\rightarrow$	Conductance
Constant real power load	$\rightarrow$	Constant real power load
Constant reactive power Element (Inductive)	$\leftrightarrow$	Constant reactive power Element (Capacitive)
Independent current source	$\rightarrow$	open
Independent voltage source	$\rightarrow$	short
Objective function gradient	$\rightarrow$	Adjoint input source

To analyze the mapping and effect of excitation sources to the adjoint network, we first consider the excitation sources of primal split-circuit $\mathcal{S}$. As it was shown in [21], [22], the sensitivities of excitation sources that set the operating point of the primal circuit $\mathcal{S}$ are zero (e.g., constant current and voltage source), and hence do not affect the adjoint circuit. Therefore, the primal excitation sources in the adjoint circuit are turned OFF, as presented in Table I. To further understand and analyze the effect of adding the excitation to the adjoint circuit, let $\boldsymbol{\psi_c}$ represent the vector of adjoint excitation sources. We can then reformulate the expression from (44) as:

$$\mathcal{J}_X^T \boldsymbol{\lambda} = \boldsymbol{\psi_c} \tag{46}$$

Next, by comparing the generalized adjoint circuit equations from (46) with the dual problem form the optimality KKT conditions given in (33), we recognize that the vector of adjoint excitation sources correspond to the negative gradient of the optimization problem, in addition to the contributions of the dual variables related to the inequality constraints. Therefore, from the circuit perspective, the negative gradient of the objective function and the dual variables related to inequality constraints represent the adjoint sources that set the operating point of the adjoint circuit in a manner that ensures controlled and optimized primal circuit operating point. For instance, consider again the n-node RLC circuit from Fig. 2. Its adjoint circuit corresponds to the conjugated RLC network and shorted voltage sources (OFF). However, it can be shown that turning the adjoint excitation voltage sources ON ensures that the current supplied by the primal voltage sources is minimized, thereby corresponding to adding the objective function of minimizing the voltage source current to the optimization problem constrained by the RLC circuit equations from Fig. 2.

With the relationship between the primal and dual problems from (33), (34) and their equivalent circuit representation established, the set of complementary slackness conditions from (35) remain to be considered. Therefore, we introduce the optimization control circuits, whose governing equations are defined by the complementary slackness conditions, which as discussed above, further set the values of the adjoint (dual) variables representing the portion of adjoint excitation sources.

Any equivalent circuit variable, including the real and reactive powers, as well as the voltage magnitude and congestion constraints given by (4), (5), (15) and (19) can be represented by the box inequality constraints. Hence, to obtain the generalized optimization control circuit representation, we perturb and reformulate the complementary slackness conditions (35), which can be written in terms of "diode-like" nonlinearities

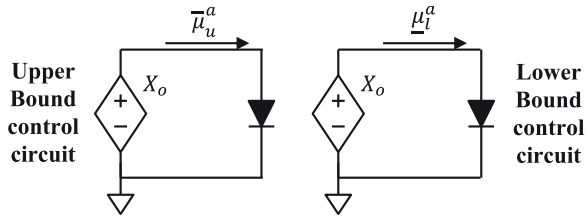

Fig. 3. Generalized control optimization circuits. Note that a diode circuit symbol only indicates the type of the circuit nonlinearity.

for uth and lth upper and lower bounds ($\bar{X}_u$, $\underline{X}_l$):

$$\bar{\mu}_u = \frac{\varepsilon}{\bar{X}_u - X_o + \bar{\mu}_{sat,u}} \quad \forall u \in \left[1, \left|\bar{I}_o\right|\right], \forall o \in [1, |\boldsymbol{X}|] \tag{47}$$

$$\underline{\mu}_l = \frac{\varepsilon}{X_o - \underline{X}_l + \underline{\mu}_{sat,l}} \quad \forall l \in [1, |\underline{I}_o|], \forall o \in [1, |\boldsymbol{X}|] \tag{48}$$

where $\bar{\mu}_u$ and $\underline{\mu}_l$ represent the uth and lth dual variables related to the respective upper and lower limits, $|\bar{I}_o|$ and $|\underline{I}_o|$ are the total number of upper and lower bounds, while $\bar{\mu}_{sat,u}$ and $\underline{\mu}_{sat,l}$ represent the upper and lower adjoint saturation currents.

Importantly, since the range $\bar{\mu}_u$ and $\underline{\mu}_l$ values can be now determined from the problem's nature and physical characteristics, the addition of saturation currents ($\bar{\mu}_{sat,u}$ and $\underline{\mu}_{sat,l}$) are similar to models for semiconductor diodes in SPICE [21]. The model discontinuity at the bound can now be eliminated by constraining the adjoint currents to be defined by the maximum physically meaningful value when the controlled variable reaches the bound. The discussion of choosing the values of adjoint saturation currents is further given in Section V. Furthermore, beside the complete removal of model discontinuities within the feasible space, a common practice in SPICE modeling of the steep nonlinearities [20], [21] is to keep the exact model only in the physical range, while approximating the "non-physical" regions by piecewise-continuous linear functions that are usually obtained as a Taylor linearization at the boundary point of physical regions. Therefore, the redefined piecewise continuous complementary slackness conditions that represent the governing equations of optimization control circuits (shown in Fig. 3) can be written as:

$$\bar{\mu}_u^a = \begin{cases} \frac{\varepsilon}{\bar{X}_u - X_o + \bar{\mu}_{sat,u}} & \text{if } X_o < \bar{X}_u \\ \frac{\varepsilon\left(\bar{\mu}_{sat,u} - \bar{X}_u\right)}{\bar{\mu}_{sat,u}^2} + \frac{\varepsilon}{\bar{\mu}_{sat,u}^2} X_o & \text{if } X_o \geq \bar{X}_u \end{cases} \tag{49}$$

$$\underline{\mu}_l^a = \begin{cases} \frac{\varepsilon}{X_o - \underline{X}_l + \underline{\mu}_{sat,l}} & \text{if } X_o > \underline{X}_l \\ \frac{\varepsilon\left(\underline{\mu}_{sat,l} + \underline{X}_l\right)}{\underline{\mu}_{sat,l}^2} - \frac{\varepsilon}{\underline{\mu}_{sat,l}^2} X_o & \text{if } X_o \leq \underline{X}_l \end{cases} \tag{50}$$

As can be seen from (49), (50), the steepness of diode nonlinearities and hence the accuracy of CS constraints is defined by an ε constant. The traditional PDIP methods define the "homotopy-like" algorithms [19] that provide more stable convergence properties with iteratively updating ε constant (barrier

parameter) until it approaches a small number at the point of convergence. However, beside the increase of iteration count during the homotopic stepping toward the original problem, the nonlinear constraint optimization problems cannot guarantee the problem feasibility on the whole homotopy path [19]. On the other side, SPICE has developed the limiting and homotopy algorithms [21] that efficiently handle the extremely steep nonlinearities (e.g., diodes, transistor switches, etc.) within circuits of enormous scale and complexity. Therefore, instead of applying the traditional PDIP algorithms to handle the steepness of the "diode-like" curves, we keep (49), (50) steep from the beginning of simulation, and modify the SPICE-style heuristics [21] to develop the Critical Curvature Region for limiting. This is discussed in further detail in Section V.

Lastly, after we showed that the complete optimization problem defined by the equivalent circuit constraints can be represented in terms of equivalent circuits and solved as an equivalent circuit problem, we define the Equivalent Circuit Programming as a new class of optimization problems.

Definition 1: (Equivalent Circuit Program - ECP). An optimization problem whose constraints can be expressed in terms of equivalent circuit equations. Therefore, the problem optimality conditions represent the governing equations of an equivalent circuit, whose operating point can be obtained by solving a circuit simulation problem. Most importantly, if sufficient conditions are met, the ECP operating point exactly represent ***an*** optimal solution of the optimization problem.

1) Generic Framework for Optimizing Power Grid: An equivalent split-circuit formulation was demonstrated to provide a generalized power system simulation framework [15]–[17], [23]–[27] that can include any physics-based model, such as induction motors [24] or power electronics [23]. Since both transmission and distribution networks can be represented by an equivalent circuit, they can be simulated (jointly [26] or separately [25]) within the same framework. Furthermore, the circuit simulation modeling methodology used in modeling the steeply nonlinear devices, such as transistor switches, can be adapted [27] to develop the continuous models of nonlinear power grid device characteristics. This includes PV/PQ conversion of the generators and shunts, as well as the transformer tap control [27]. Most importantly, the globally convergent heuristics that are relied upon in SPICE can be adapted to ensure the robust convergence properties of the developed nonlinear models [21], [27].

Lastly, since each of the split-circuit models are further defined within the adjoint domain, the proposed framework for modeling and solving the optimal power flow problem can be generalized to incorporate any physics-based models. For the AC-OPF problem specifically, we derive the ECP model of a generator that contains the embedded objective function gradient within the model. This further ensures the minimized generated real power solution.

2) AC-OPF Circuit Model of a Generator: The complex governing equations of a generator model and the respective real and reactive power constraints are given in (10) and (15), (16). The powerflow circuit for the generator in terms of admittance state variables is derived by splitting (10) into its real and imaginary currents $I_{GR,g}$ and $I_{GI,g}$:

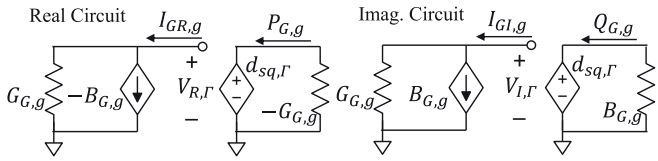

Fig. 4. Powerflow equivalent circuit of a generator.

$$I_{GR,g} = G_{G,g}V_{R,\Gamma} - B_{G,g}V_{I,\Gamma} \quad \forall g \in \mathcal{G} \tag{51}$$

$$I_{GI,g} = G_{G,g}V_{I,\Gamma} + B_{G,g}V_{R,\Gamma} \quad \forall g \in \mathcal{G} \tag{52}$$

Moreover, the real and reactive power constraints are represented by the two additional equivalent circuits as in Fig. 4, where the powers are proportional to the currents flowing through the voltage source set by the bus voltage magnitude.

We start the derivation of adjoint power flow circuit by finding the first order sensitivity $\mathcal{J}_g(\boldsymbol{X})$ matrix of the GB generator governing equations that satisfies (42):

$$\mathcal{J}_g(\boldsymbol{X}) = \begin{bmatrix} G_{G,g} & -B_{G,g} & V_{R,\Gamma} & -V_{I,\Gamma} & 0 & 0 & 0 \\ B_{G,g} & G_{G,g} & V_{I,\Gamma} & V_{R,\Gamma} & 0 & 0 & 0 \\ 0 & 0 & d_{sq,\Gamma} & 0 & 1 & 0 & G_{G,g} \\ 0 & 0 & 0 & -d_{sq,\Gamma} & 0 & 1 & -B_{G,g} \end{bmatrix} \tag{53}$$

To further set the operating point of the adjoint power flow circuit that ensures that the real power supplied by the generator is minimized as well as bounded by the power control circuits, the governing equations of generator adjoint circuit can be written from established relationships in (33) and (46) as:

$$\mathcal{J}_g(\boldsymbol{X})^T \begin{bmatrix} \lambda_{R,\Gamma} \\ \lambda_{I,\Gamma} \\ \lambda_{P,g} \\ \lambda_{Q,g} \end{bmatrix} + \begin{bmatrix} 0 & 0 & 0 & 0 \\ 0 & 0 & 0 & 0 \\ 0 & 0 & 0 & 0 \\ 0 & 0 & 0 & 0 \\ 1 & -1 & 0 & 0 \\ 0 & 0 & 1 & -1 \\ 0 & 0 & 0 & 0 \end{bmatrix} \begin{bmatrix} \bar{\mu}_{P,g} \\ \underline{\mu}_{P,g} \\ \bar{\mu}_{Q,g} \\ \underline{\mu}_{Q,g} \end{bmatrix} = -\frac{\partial \mathcal{F}_c}{\partial \boldsymbol{X}} \tag{54}$$

where $\lambda_{R,\Gamma}$ and $\lambda_{I,\Gamma}$ represent the adjoint voltages, $\bar{\mu}_{P,g}$, $\underline{\mu}_{P,g}$, $\bar{\mu}_{Q,g}$ and $\underline{\mu}_{Q,g}$ are the dual variables related to upper and lower bounds of real and reactive powers respectively, while $\lambda_{P,g}$ and $\lambda_{Q,g}$ are the LMPs related to real and reactive powers.

The first two equations from (54) represent the main adjoint split-circuit governing equations of a generator. By letting the real and imaginary adjoint currents ($\Im_{GR,g}$ and $\Im_{GI,g}$) be a function of currents at the generator output terminal, we further write the nonlinear adjoint split-circuit currents of a generator:

$$\Im_{GR,g} = G_{G,g}\lambda_{R,\Gamma} + B_{G,g}\lambda_{I,\Gamma} \quad \forall g \in \mathcal{G} \tag{55}$$

$$\Im_{GI,g} = G_{G,g}\lambda_{I,\Gamma} - B_{G,g}\lambda_{R,\Gamma} \quad \forall g \in \mathcal{G} \tag{56}$$

Note that the currents from (55), (56) define the adjoint admittance of the generator GB model, as shown by Table I. Most

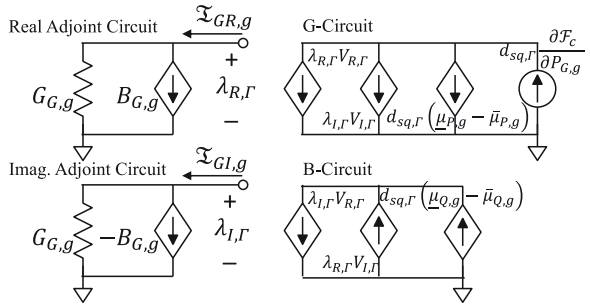

Fig. 5. Adjoint powerflow circuit of a generator that supplies optimal real power, enforced by embedded to objective function gradient to G-Circuit.

importantly, the use of power flow and adjoint generator currents is the typical practice in equivalent circuit modeling. *The respective currents are not the variables of the formulation, but rather an aggregation of the rest of the system, for which governing equations are built by hierarchically combining the respective circuit models of the simulation problem.*

The next four equations from (54) are given as:

$$V_{R,\Gamma}\lambda_{R,\Gamma} + V_{I,\Gamma}\lambda_{I,\Gamma} + d_{sq,\Gamma}\lambda_{P,g} = 0 \qquad \forall g \in \mathcal{G} \qquad (57)$$

$$V_{R,\Gamma}\lambda_{I,\Gamma} - V_{I,\Gamma}\lambda_{R,\Gamma} - d_{sq,\Gamma}\lambda_{Q,g} = 0 \qquad \forall g \in \mathcal{G} \qquad (58)$$

$$\lambda_{P,g} = \underline{\mu}_{P,g} - b_g - 2c_g P_{G,g} - \bar{\mu}_{P,g} \qquad \forall g \in \mathcal{G} \qquad (59)$$

$$\lambda_{Q,g} = \underline{\mu}_{Q,g} - \bar{\mu}_{Q,g} \qquad \forall g \in \mathcal{G} \qquad (60)$$

To further reduce the variable count of the AC-OPF circuit, we can eliminate the Lagrange multipliers related to the real and reactive powers ($\lambda_{P,g}$ and $\lambda_{Q,g}$) by substituting (59), (60) into (57), (58) respectively. This which further yields the constraints added to ensure the optimality and control of the powers supplied by the conductance and susceptance state variables, governing the G-circuit and B-circuit from Fig. 5. The nonlinear adjoint powerflow circuit of a generator that maps (55), (56) and (57)–(60) is shown in Fig. 5.

It is important to note that the derived governing circuit equations precisely represent the part of KKT conditions contributed to the generator modeling constraints. Hence, to solve the nonlinear circuit simulation problem, each of the nonlinear primal and adjoint circuit equations are linearized by means of the first order Taylor expansion [15]–[17] to obtain the linearized ECP circuit models that are then combined together to build to complete ECP representation of AC-OPF problem.

3) Building and Solving an Equivalent Circuit Program: The complete ECP circuit representation is obtained by hierarchically combining (connecting) the primal, adjoint and control circuit models, as defined by the grid (network) topology. It is important to note that the hierarchical building of the circuit representation corresponds to a modular construction of the Jacobian/Hessian matrix and constant vector that defines the Newton Raphson values during the iteration process.

Once the complete equivalent split-circuit is built, its set of governing circuit equations correspond to the nonlinear set of KKT optimality conditions as linearized by a first order Taylor expansion. This linearization represents that step for the inner most loop of the Newton Raphson method. Since iteratively solving the circuit simulation problem corresponds to Newton Raphson iterations, at every iteration only circuit elements (Jacobian/Hessian terms) that are dependent on the values from the previous iteration are rebuilt, while the linear parts are built once at the beginning of the simulation. This approach was shown to represent an extremely efficient formulation and solution method for solving nonlinear circuit problems [18], [21]. The main difference between the circuit simulation and traditional methods, however, is the circuit formalism obtained from the circuit representation of the problem. This provides important information that allows for developing efficient heuristics to ensure the robust convergence properties and scalability directly from the physical characteristics of the problem, as further discussed in the following section.

V. Enhanced Simulation of Circuit-Based AC-OPF Problem Equivalent (ESCAPE) Approach

Solving the nonlinear constrained optimization (NCO) problem can be a very challenging task that is prone to divergence or very slow convergence. These challenges can arise due to the inefficient handling of nonlinear constraints combined with modeling of inequality constraints. One of the widely used methods for solving the NCO problems, Primal Dual Interior Point (PDIP) method [19], tackles those challenges by multiplying the entire solution vector with the smallest damping factor needed to maintain the iteration as feasible and further decrease the error. However, since the first introduction of the SPICE-like simulators [20], it has been shown that damping the complete solution vector of a nonlinear simulation has two serious drawbacks [20]. First, if the iterative solutions are in vicinity of the correct solution, the convergence process is unnecessarily slowed down. Second, if the solutions of two consecutive iterations differ widely, the problem may diverge or oscillate. Importantly, from the perspective of optimization problem, the unnecessary damping of certain variables from a complete solution vector can force the iteration process to remain stuck in the local area, hence increases the chances of converging to a local solution or a saddle point. Therefore, instead of applying the traditional PDIP algorithms to solve the AC-OPF circuit, we use the idea of modeling the complementary slackness conditions as in PDIP and combine it with a circuit simulation solution approach to the problem to derive a new simulation technique.

Herein, we introduce our Enhanced Simulation of Circuit-based AC-OPF Problem Equivalent (ESCAPE) approach as an adaptation of limiting heuristics from circuit simulations.

A limiting technique can be generalized as follows: for a given maximum step size vector $\Delta\boldsymbol{\Upsilon}_{\max}$, we can find the vector of damping factors ($\boldsymbol{\delta_C}$) that limits the NR variable update as:

$$\boldsymbol{\delta_C} = \min\left\{\boldsymbol{e}, [\operatorname{sign}(\Delta\boldsymbol{\Upsilon}) \odot \Delta\boldsymbol{\Upsilon}_{\max}] \oslash \Delta\boldsymbol{\Upsilon}\right\} \qquad (61)$$

$$\boldsymbol{\Upsilon}^{k+1} = \boldsymbol{\Upsilon}^{k} + \boldsymbol{\delta_C} \odot \Delta\boldsymbol{\Upsilon} \qquad (62)$$

where $\oslash$ represent the pointwise division, $\boldsymbol{e}$ is a vector of ones, and $\boldsymbol{\Upsilon}$ is a placeholder vector of limited variables. Note from

(61) that in contrast to the traditional damping approaches, each of the variables herein can have its own limiting factor.

A. Voltage Limiting

Voltage Limiting was shown be a simple and effective simulation technique that limits the value of the step change that the real and imaginary voltage vectors are allowed to make during each NR iteration in powerflow problem [16], [17]. For the AC-OPF circuit, the voltage limiting is done in two stages. In the first one, we limit the powerflow real and imaginary voltage steps, i.e., $\boldsymbol{\Upsilon} \in \{\boldsymbol{V_R}, \boldsymbol{V_I}\}$ as in (61) and use the obtained damping vectors to limit the real and imaginary adjoint voltages respectively. To further ensure that the step sizes of adjoint voltages do not exceed the predefined limits, the second stage applies limiting technique to adjoint voltages.

B. Admittance Limiting

As discussed in [16], the voltages of powerflow equivalent circuit are very sensitive to the reactive power change during nonlinear iteration. Hence, we redefine the Q limiting [16], [17] to limit the NR step change of the admittance state variables of the generator model. With well-defined bounds on admittance state variables from the bounds on real and reactive power and voltage magnitude, we establish the maximum step change vectors for the generator conductance and susceptance:

$$\Delta \boldsymbol{G}_{max} = \alpha \left(\boldsymbol{G}_{max} - \boldsymbol{G}_{min} \right) \tag{63}$$

$$\Delta \boldsymbol{B}_{max} = \alpha \left(\boldsymbol{B}_{max} - \boldsymbol{B}_{min} \right) \tag{64}$$

where $\alpha \in (0, 1]$ represent the discretizing factor.

C. Critical Curvature Region (CCR) Limiting

In contrast to the feasible range of the power flow split-circuit variables that are normalized and well defined by the bounds of the optimization problem, the set of adjoint variables, particularly the ones related to problem bounds, may not be well bounded in general. However, as shown in Section III, the gradient of the objective function represents an excitation source of the adjoint circuit, and thereby determines its operating point. Therefore, in order to prevent the large variations of dual variables, the first step in obtaining the efficient limiting heuristics is normalizing the adjoint circuit.

1) Normalizing the Adjoint Circuit: Consider a quadratic cost function from (1) that is defined by the set of cost function coefficients $\{\boldsymbol{a}, \boldsymbol{b}, \boldsymbol{c}\}$. Herein, we introduce the adjoint per unit normalization (a.p.u.) of the adjoint excitation sources; i.e., gradient of the objective function (Section III). Importantly, since scaling of the cost function by a positive constant doesn't affect its minima, we obtain the base-factor that normalizes the objective function as:

$$b_{apu} = \max \left[\max \left(\boldsymbol{b}, 2\boldsymbol{c} \right) \right] \tag{65}$$

The normalized objective function now sets the adjoint circuit operating point in the range of around 1 a.p.u. Therefore, the values of dual variables set by the upper and lower bound

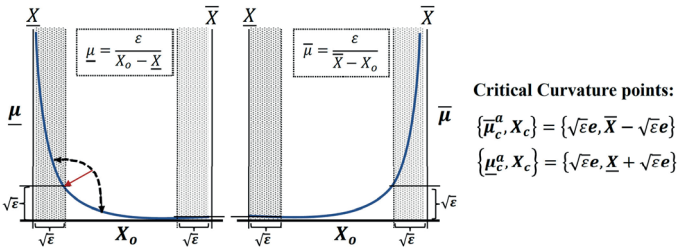

Fig. 6. Defining the Critical Curvature regions.

complementary slackness constraints correspond to the per unit amount of injected adjoint current needed to control the respective primal variables. Hence, choosing the value of saturation adjoint currents from (49), (50) that yield the 40 a.p.u. dual currents at the boundary is sufficient as the upper bound on physical region of dual variables.

2) Critical Curvature Regions: The Critical Curvature regions (CCR) can be defined based on the maximum curvature points of complementary slackness functions (49), (50) as shown in Fig. 6. Hence, instead of damping the primal and dual variables of the complementary slackness conditions over their entire domain, the diode heuristics [20], [21] are adapted to limit the NR step sizes only if the current iterates are within the defined CCRs and exceed the predefined threshold step.

3) Adaptation of Diode Alternating Basis Technique [21]: To ensure the efficient convergence properties of the steep nonlinearities within CCRs (see Fig. 6), as well as preserve the feasibility of the ECP circuit operating point, we modify the circuit simulation heuristics used in solving diode circuits [18], [20], [21]. This approach was found to be nearly optimal for limiting the diode circuits in SPICE [20]. The alternating basis limiting technique is obtained [21] by equating the nonlinear function value at $(k+1)$th iteration with its linearized Taylor approximation evaluated using the nonlimited NR step, ΔX_o, as shown in (66), (67).

$$\frac{\varepsilon}{\bar{X}_u - X_o^{k+1} + \bar{\mu}_{sat,u}} = \frac{\varepsilon + \bar{\mu}_u^{a,k} \Delta X_o}{\bar{X}_u - X_o^k + \bar{\mu}_{sat,u}} \quad \forall u \in \left[1, \left|\bar{I}_o\right|\right] \tag{66}$$

$$\frac{\varepsilon}{X_o^{k+1} - \underline{X}_l + \underline{\mu}_{sat,l}} = \frac{\varepsilon - \underline{\mu}_l^{a,k} \Delta X_o}{X_o^k - \underline{X}_l + \underline{\mu}_{sat,l}} \quad \forall l \in [1, |\underline{I}_o|] \tag{67}$$

After solving for X_o^{k+1} we obtain its NR step limiting expressions that are applied within the CCR regions:

$$X_o^{k+1} = \bar{X}_u + \bar{\mu}_{sat,u} - \frac{\varepsilon}{\varepsilon + \bar{\mu}_u^{a,k} \Delta X_o} \left(\bar{X}_u + \bar{\mu}_{sat,u} - X_o^k \right) \tag{68}$$

$$X_o^{k+1} = \underline{X}_l - \underline{\mu}_{sat,l} + \frac{\varepsilon}{\varepsilon - \underline{\mu}_l^{a,k} \Delta X_o} \left(X_o^k - \underline{X}_l + \underline{\mu}_{sat,l} \right) \tag{69}$$

Finally, to prevent oscillation for small values of ε, we ensure that if current step makes the next iterate go from a CCR to

neutral region or vice versa, we limit it such that it has to stop at the maximum curvature point before entering a new region.

D. Embedding the Homotopy Within the ECP Circuit

To allow the robust convergence of any large-scale power system optimization problem, we extend the Tx-stepping homotopy method [16], [27] to the adjoint domain. The solution of the optimal power flow is obtained by embedding the homotopy factor $\eta \in [0, 1]$ to linear series and shunt network elements and transformer model, as shown in (70)–(72). The system equations are then sequentially solved via the relaxed ECP problems while gradually decreasing the homotopy factor to zero from one. Namely, for the initial homotopy factor set to one, the ECP circuit is virtually "shorted." Now, the optimal power flow solution corresponds to the economic dispatch solution and can be trivially obtained under the assumption that there is sufficient generation in the system to supply the load. Gradually decreasing the embedded homotopy factor η to zero sequentially relaxes the ECP circuit toward its original state, while using the solution from the previous sub-problem to initialize the ECP circuit for the next homotopy decrement:

$$G_L + jB_L = (\eta\Upsilon + 1)(G_L + jB_L) \tag{70}$$

$$t(\eta) = t + (1 - t)\eta \tag{71}$$

$$\theta_{ph}(\eta) = (1 - \eta)\theta_{ph} \tag{72}$$

where Υ represents an admittance scaling factor, t is the transformer tap, and θ_{ph} is the phase shifting angle.

E. Towards a Globally Convergent AC-OPF Algorithm

Years of research in the circuit simulation field have advanced the techniques of Newton Raphson step limiting and application of homotopy methods that are shown to exhibit global convergence properties [18], [21]. We have shown that the same heuristics can be adapted and extended to the power system simulation problems, thereby guaranteeing similar global convergence properties [17], [26], [27]. Furthermore, by strictly removing the discontinuities of the complementary slackness conditions (49), (50) and with extension of the power flow heuristic and homotopy algorithms to the adjoint (dual) domain, it can be demonstrated that if a feasible solution does exist, the circuit simulation techniques can bound the NR step while maintaining the full rank solution matrix throughout the simulation [27]. It follows that the same robust convergence properties remain within the ECP problems, such as AC-OPF.

VI. Simulation Results

The circuit element library for the derived models that map the AC-OPF problem was built and incorporated in MATLAB to implement the ESCAPE algorithm. The tool reads in the 'mpc' input file, translates the parsed information into the circuit parameters, hierarchically builds the sparse circuit equations by combining the circuit models that correspond to building the set of KKT conditions, and then iteratively solves them to find the operating point of the AC-OPF circuit. In addition to the nonlinear circuit simulator, a linear simulator is used to initialize the adjoint split-circuit. All the simulations were run on MacBook Pro 2.9 GHz Intel Core i7.

We demonstrate the robustness of our circuit formulation based approach by evaluating the following: 1) *IEEE pglib and PEGASE test cases libraries*; 2) *local optimal solutions test cases from* [5]; 3) *GridPack data set library from PNLL*; and 4) Synthetic Eastern Interconnection test case [29]. The problems were *initialized using the real power and the voltage angle obtained from a DC-OPF solution that includes a flat start for voltage magnitudes and reactive powers given by the mean values defined by respective limits*. Each of the test cases is solved for current congested (upper bound on maximum current magnitude of transmission line) and nominal operating conditions (without congestion constraints). We compare the results for our ECP formulation with the 'PQV' AC-OPF and relaxed 'SDP' AC-OPF formulations solved with 'MIPS'/'FMINCON' and 'SDPT3' toolboxes by using the default input solver parameters, (maximum constraint violation 5E-6, optimality tolerance 1E-4, variable tolerance of 1E-4 p.u. and a maximum iteration count of 500 iterations) within the MATPOWER solver. The results are summarized in Table II.

The ESCAPE technique obtained a solution for all of the examined test cases during both operating conditions and converged to the same optimal solution point for each case (Table II) starting from both DC-OPF and input file initial starts. In contrast, the MATPOWER 'MIPS' solver failed on several of the testcases, notably the larger size systems, and the 'FMINCON' toolbox performed better in those cases, but also diverged for the two smaller cases when initialized from DC-OPF. For this reason, we present the MATPOWER results as initialized from DC-OPF and test case input file separately. Lastly, the SDP relaxation performed as reported in the literature [5], [12], and it was characterized by slower runtimes than the other approaches. Furthermore, the SDP relaxation failed to converge for the test cases that are known to have multiple local solutions and was able to successfully find the global solutions of the 14, 30 and 89 bus test cases that match the solutions obtained from ESCAPE and MATPOWER.

We next analyze the ESCAPE runtime as a function of system size and compare it to the other formulations in Fig. 7. All cases were run under congested operating conditions for the same default parameters. The 'PQV' AC-OPF formulation is run with both 'MIPS' and 'FMINCON' solvers, and the better of the two run times is reported. As it can be seen from Fig. 7, ESCAPE demonstrated better robustness with problem size. We believe that this can be attributed, in part, to exploiting the "problem physics" to limit only specific variables that can cause divergence, just as is done in SPICE [18], [20], [21]. This is in contrast to general purpose optimization solvers, such as PDIP methods, that uniformly limit the solver step size, while homotopically varying the ε-parameter. Importantly, even though the problem size is slightly increased in comparison to the traditionally formulated AC-OPF, the physics-based heuristics decrease the iteration count, and when combined with the sparse circuit methodology of building the circuit equations, improve the

TABLE II
AC-OPF SIMULATION RESULTS: COMPARING THE PROPOSED CIRCUIT FORMULATION WITH THE TRADITIONAL ONES

Cat.	Test case	AC-OPF Circuit Formulation + ESCAPE		MATPOWER AC-OPF with DC-OPF start		MATPOWER AC-OPF with input file start	
		Nominal operation	*Congested operation*	*Nominal operation*	*Congested operation*	*Nominal operation*	*Congested operation*
		Cost [$/hr]	**Cost [$/hr]**	**Cost [$/hr]**	**Cost [$/hr]**	**Cost [$/hr]**	**Cost [$/hr]**
2	*Case 9mod*	3,087.84	3,087.84	3,087.85 **	4,246.5 (MIPS)/3,087.8	3,087.84 **	4,246.5 (MIPS)/3,087.8
1	*Case 14*	11,230.52	11,230.52	11,230.52	11,230.52	11,230.52	11,230.52
1	*Case 30*	10,598.21	11,708.23	10,598.21	11,708.23	10,598.21	11,708.23
2	*Case 39mod2*	941.74	941.74	941.74	941.74 **	941.74	941.74 **
2	*Case 39mod3*	1,888.76	1,894.05	1,888.76 **	1,894.05 **	1,888.76 **	1,894.05 **
1	*Case 89*	5,817.60	5,817.60	5,817.60	5,817.60	5,817.60	5,817.60
2	*Case 118mod*	129,625.02	129,625.02	129,625.02	129,625.03 (MIPS)/DIVERGE	129,625.02	129,625.02
1	*Case 300*	638,312.01	657,418.35	638,312.01	657,418.35	638,312.01	657,418.35
2	*Case 300mod*	378,540.49	378,540.49	378,540.49 (MIPS)/DIVERGE	378,540.49 (MIPS)/DIVERGE	378,540.49	378,540.50
1	*Case 1354*	74,060.41	74,064.30	74,060.41	74,064.30	74,060.41	74,064.30
1	*Case 2869*	133,980.72	133,993.48	133,980.72	133,993.48	133,980.72	133,993.48
1	*Case 9241*	315,886.40	***315,902.49*** ⋆	*315,888.48* **	315,903.4 (MIPS)/315,902.8	315,886.40**	315,903.36
1	*Case 13659*	***386,106.58*** ⋆	***386,106.58*** ⋆	--- §	--- §	--- §	--- §
3	*Case 40605*	15,099,595.29	***15,395,681.29*** ⋆	---	---	15,099,595.30 **	15,395,683.29 **
3	*Case 68251*	***26,960,544.97*** ⋆	***27,551,688.77*** ⋆	---	---	26,960,547.17 **	---
4	*SyntheticUSA*	16,439,446.70	16,439,446.70	16,441,143.10**	16,439,446.70**	16,439,446.70 **	16,439,446.70 **

— Test case didn't converge after maximum iteration count (500) is reached with both 'MIPS' and 'FMINCON'.
⋆ Lower optimal cost found by ESCAPE. The obtained optimal solution is further validated by using it as an initial start for running the AC-OPF in MATPOWER.
** 'MIPS' MATPOWER solver diverged or didn't converge after one hour; optimal solution obtained using 'FMINCON' toolbox.
§ Case13659 did not run with both 'MIPS' and 'FMINCON' solvers in MATPOWER, however, authors in [30] have reported the solution obtained using 'KNITRO' given as: $386,107.5 for both operating conditions.

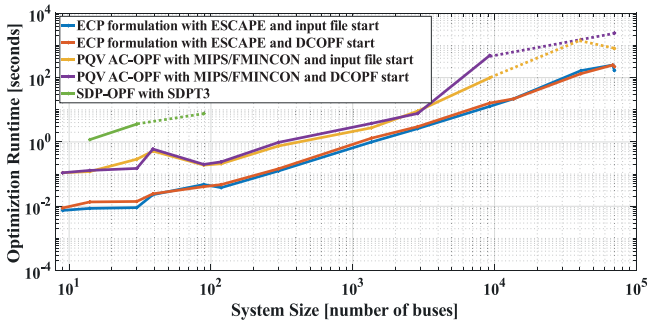

Fig. 7. Optimization runtime comparison.

simulation efficiency. These results, however, do not exclude that the other toolboxes may perform better, but rather indicate a promising path toward developing a generalized and robust framework for solving the power grid optimizations solely from the physical characteristics of the problem.

VII. CONCLUSION

In this paper we introduced an equivalent circuit formulation for modeling and solving the AC-OPF problem. A new macro-model of a generator was defined in terms of conductance and susceptance state variables. The linear adjoint circuit theory was extended to include the nonlinearities at fixed frequency and further allow the direct mapping of KKT optimality conditions to a circuit simulation problem. The preliminary simulation results show that understanding of physics behind the ECP circuits helps in achieving stable and efficient convergence properties and provides greater probability of converging to optimal solution with lower cost function values. Most importantly, the framework is scalable to realistic large-scale power systems and facilitates incorporation of any physics-based power grid device models.

REFERENCES

[1] W. F. Tinney and C. E. Hart, "Power flow solutions by Newton's method," *IEEE Trans. Power App. Syst.*, vol. PAS-86, no. 11, pp. 1449–1460, Nov. 1967.
[2] J. Carpentier, "Contribution to the economic dispatch problem," *Bull. Soc. Francaise Electriciens*, vol. 8, pp. 431–447, 1962.
[3] H. W. Dommel and W. F. Tinney, "Optimal power flow solutions," *IEEE Trans. Power App. Syst.*, vol. PAS-87, no. 10, pp. 1866–1876, Oct. 1968.
[4] M. B. Cain, R. P. O'Neill, and A. Castillo, "History of optimal power flow and formulations, OPF Paper 1," Federal Energy Regulatory Commission, Washington, D.C., USA, Tech. Rep. 1, Dec. 2012.
[5] W. A. Bukhsh, A. Grothey, K. I. M. McKinnon, and P. A. Trodden, "Local solutions of optimal power flow problem," *IEEE Trans. Power Syst.*, vol. 28, no. 4, pp. 4780–4788, Nov. 2013.
[6] I. M. Nejdawi *et al.*, "An efficient interior point method for SQP based optimal power flow," *IEEE Trans. Power Syst.*, vol. 15, no. 4, pp. 1179–1183, Nov. 2000.
[7] R. A. Jabr, "Optimal power flow using an extended conic quadratic formulation," *IEEE Trans. Power Syst.*, vol. 23, no. 3, pp. 1000–1008, Aug. 2008.
[8] J. Lavaei and S. H. Low, "Zero duality gap in optimal power flow problem," *IEEE Trans. Power Syst.*, vol. 27, no. 1, pp. 92–107, Feb. 2012.
[9] R. A. Jabr, "Radial distribution load flow using conic programming," *IEEE Trans. Power Syst.*, vol. 21, no. 3, pp. 1458–1459, Aug. 2006.
[10] S. Sojoudi and J. Lavaei, "Physics of power networks makes hard optimization problems easy to solve," in *Proc. IEEE PES Gen. Meeting*, 2012, pp. 1–8.
[11] R. Madani, S. Sojoudi, and J. Lavaei, "Convex relaxation for optimal power flow problem: Mesh networks," *IEEE Trans. Power Syst.*, vol. 30, no. 1, pp. 199–211, Jan. 2015.
[12] B. C. Lesieutre *et al.*, "Examining the limits of the application of semidefinite programming to power flow problems," in *Proc. 49th Annu. Allerton Conf. Commun. Control Comput.*, 2011, pp. 1492–1499.
[13] W. M. Lin, T.-S. Zhan, and M.-T. Tsay, "Multiple–frequency three-phase load flow for harmonic analysis," *IEEE Trans. Power Syst.*, vol. 19, no. 2, pp. 897–904, May 2004.
[14] W. M. Lin, C. H. Huang, and T. S. Zhan, "A hybrid current-power optimal power flow," *IEEE Trans. Power Syst.*, vol. 23, no. 1, pp. 177–185, Feb. 2008.
[15] M. Jereminov, D. M. Bromberg, L. Xin, G. Hug, and L. Pileggi, "Improving robustness and modeling generality for power flow analysis," in *Proc. IEEE Transmiss. Distrib. Conf. Expo.*, 2016, pp. 1–5.
[16] A. Pandey, M. Jereminov, G. Hug, and L. Pileggi, "Improving power flow robustness via circuit simulation methods," *IEEE Power Energy Soc. Gen. Meeting*, Chicago, IL, USA, 2017, pp. 1–5.

[17] A. Pandey, M. Jereminov, M. Wagner, G. Hug, and L. Pileggi, "Robust convergence of power flow using T-x stepping method with equivalent circuit formulation," in *Proc. Power Syst. Comput. Conf.*, Dublin, Ireland, 2018, pp. 1–7.
[18] L. Pileggi, R. Rohrer, and C. Visweswariah, *Electronic Circuit & System Simulation Methods*. New York, NY, USA: McGraw-Hill, 1995.
[19] S. Boyd and L. Vandenberghe, *Convex Optimization*. New York, NY, USA: Cambridge Univ. Press, 2004.
[20] L. Nagel and R. Rohrer, "Computer analysis of nonlinear circuits, excluding radiation (CANCER)," *IEEE J. Solid-State Circuits*, vol. SSC-6, no. 4, pp. 166–182, Aug. 1971.
[21] W. J. McCalla, *Fundamentals of Computer-Aided Circuit Simulation*. Boston, MA, USA: Kluwer, 1988.
[22] S. W. Director and R. Rohrer, "The generalized adjoint network and network sensitivities," *IEEE Trans. Circuit Theory*, vol. 16, no. 3, pp. 318–323, Aug. 1969.
[23] M. Jereminov, A. Pandey, D. M. Bromberg, X. Li, G. Hug, and L. Pileggi, "Steady-state analysis of power system harmonics using equivalent split-circuit models," in *Proc. Innov. Smart Grid Technol. Conf. Eur.*, Ljubljana, Slovenia, Oct. 2016, pp. 1–6.
[24] A. Pandey, M. Jereminov, X. Li, G. Hug, and L. Pileggi, "Unified power system analyses and models using equivalent circuit formulation," in *Proc. IEEE Power Energy Soc. Innov. Smart Grid Technol.*, Minneapolis, St. Paul, USA, 2016, pp. 1–5.
[25] M. Jereminov, D. M. Bromberg, A. Pandey, X. Li, G. Hug, and L. Pileggi, "An equivalent circuit formulation for three-phase power flow analysis of distribution systems," in *Proc. IEEE Transmiss. Distrib. Conf. Expo.*, Dallas, TX, USA, 2016, pp. 1–5.
[26] A. Pandey, M. Jereminov, M. Wagner, D. M. Bromberg, G. Hug, and L. Pileggi, "Robust power flow and three phase power flow analyses," *IEEE Trans. Power Syst.*, vol. 34, no. 1, pp. 616–626, Jan. 2019, doi: 10.1109/TPWRS.2018.2863042.
[27] A. Pandey, "Robust steady-state analysis of power grid using equivalent circuit formulation with circuit simulation methods," Doctoral thesis, Dept. Elect. Comput. Eng., Carnegie Mellon Univ., Pittsburgh, PA, USA, Aug. 2018.
[28] D. K. Molzahn and L. A. Roald, "Towards an AC optimal power flow algorithm with robust feasibility guarantees," in *Proc. Power Syst. Comput. Conf.*, 2018, pp. 1–7. [Online]. Available: https://molzahn.github.io/pubs/molzahn_roald-acopf_robust2018.pdf
[29] A. B. Birchfield, T. Xu, and T. Overbye, "Power flow convergence and reactive power planning in creation of large synthetic grids," *IEEE Trans. Power Syst.*, vol. 33, no. 6, pp. 6667–6674, Nov. 2018.
[30] C. Josz *et al.*, "AC power flow data in MATPOWER and QCQP format: iTesla RTE snapshots and PEGASE," ArXiv, 1603.01533, Mar. 2016.

Marko Jereminov (M'15) was born in Belgrade, Serbia. He received the B.Sc. degree in electrical engineering from South Carolina State University, South Carolina, USA, in 2016, and is currently working toward the Ph.D. degree in electrical and computer engineering at Carnegie Mellon University, Pittsburgh, PA. He previously interned at Pearl Street Technologies, Pittsburgh, as well as at the Department of Electrical and Computer Engineering, Carnegie Mellon University, prior to joining as a Ph.D. student. His research interests include optimization, simulation, and modeling of electrical power systems.

Amritanshu Pandey was born in Jabalpur, India. He received the M.Sc. degree in electrical engineering from Carnegie Mellon University, Pittsburgh, PA, in 2012, where he is currently working toward the Ph.D. degree. Prior to joining as a doctoral student at Carnegie Mellon University, he was an Electrical Engineer with MPR Associates, Inc., from 2012 to 2015. He has previously interned at Pearl Street Technologies, ISO New-England and GE Global Research. His research interests include modeling and simulation, optimization and control of power systems.

Larry Pileggi (F'02) received the Ph.D. degree in electrical and computer engineering from Carnegie Mellon University in 1989. He is the Tanoto Professor of electrical and computer engineering with Carnegie Mellon University, and has previously held positions at the Westinghouse Research and Development and the University of Texas at Austin. He has consulted for various semiconductor and EDA companies, and was the Co-founder of Fabbrix, Inc., Extreme DA, and Pearl Street Technologies. He is a Co-Author of *Electronic Circuit and System Simulation Methods* (McGraw-Hill, 1995) and *IC Interconnect Analysis* (Kluwer, 2002). He has authored or coauthored more than 300 conference and journal papers and holds 40 U.S. patents. His research interests include various aspects of digital and analog integrated circuit design and design methodologies, and simulation and modeling of electric power systems. Dr. Pileggi was a recipient of various awards, including Westinghouse Corporation's highest engineering achievement award, the 2010 IEEE Circuits and Systems Society Mac Van Valkenburg Award, and the 2015 Semiconductor Industry Association University Researcher Award.